

Analytical model for collision probability assessments with large satellite constellations

Eduardo Maria Polli^a, Juan Luis Gonzalo^a, Camilla Colombo^a

^aPolitecnico di Milano, Via La Masa 34, 20158 Milan, Italy

Abstract

At a time when space debris are already a growing issue in the space sector, the deployment of large constellations, made of hundreds to thousands of satellites, is of concern from an environmental point of view. In the next decade, the space sector will undergo a considerable change as the population of active satellites is about to quintuple. This scenario will pose new challenges regarding space traffic management, generating the demand for more powerful and efficient analysis tools.

In this study, an analytical model for collision probability assessments between de-orbiting or injecting space objects and satellite constellations is presented. Considering the first to be subjected to a continuous tangential acceleration, its spiraling motion would result in a series of close approaches in the proximity of a constellation. The mathematical description of the crossing dynamics relies on the assumption of circular orbits and independent collision probabilities, but does not require to propagate the satellites' orbit and it is suitable also for elliptical crossing orbits. The statistical model presented in the current work constitutes an efficient tool for the evaluation of the mean collision probability related to this type of events. A comparison with a conventional propagation method has been performed for validation purposes.

The statistical model has been used to assess the risk connected to constellation's satellites replacement, once they have reached their programmed End-of-Life. The environmental impact of the full replacement of 12 approved constellations is analysed by means of average collision probability. In particular, it is shown that the key features for space exploitation sustainability are the maximum propulsion available from the thruster, the selection of an optimal crossing orbit and the true anomaly phases between constellations' and crossing satellites. The consequences of an in-orbit collision are also investigated by assessing the collision risk generated by the formation of a debris cloud.

The results corroborate the need for international standards for space traffic management as an exponentially increasing satellites population could trigger a chain reaction of collisions, making LEO inaccessible for decades.

© 2022 COSPAR. Published by Elsevier Ltd All rights reserved.

Keywords: Analytical Model; Collision Probability; Satellite Constellation; shell-crossing event; Tangential Low-Thrust

1. Introduction

The exponential growth the private space sector experienced in the last decade led to an improvement of the engineering knowledge and, eventually, to a reduction of the cost of payload launch per kg. This, along with the more widespread use of cellphones and Internet among the population, allowed the realization of telecommunications satellite constellations. Space-

based world-wide telecommunications could play a key role as the cost of the infrastructures related to on-ground Internet connections has left many rural and underdeveloped regions unserved. Indeed, large constellations appear to be the most suitable option to bridge the digital divide, which is one of the UN Sustainable Development Goals. Moreover, for the first time, near global coverage would be available with only one provider. In particular, SpaceX (FCC, 2018-2021), OneWeb (FCC, 2020a), Telesat (FCC, 2020b) and Amazon (FCC, 2019) plan to deploy large constellations composed by thousands of satellites within the next years, all four projects being already approved

Email addresses: eduardo.polli94@gmail.com (Eduardo Maria Polli), juanluis.gonzalo@polimi.it (Juan Luis Gonzalo), camilla.colombo@polimi.it (Camilla Colombo)

by the Federal Communications Commission (FCC), the authority responsible for spectrum usage and for launch approval, along with the Federal Aviation Administration (FAA), in the United States.

As most Internet services require fast links, satellite constellations for telecommunication purposes are going to be deployed in Low Earth Orbit (LEO). The main advantage of LEO constellations with respect to higher-altitude satellite telecommunication systems, is the low latency due to the shorter satellite-Earth distances involved. The latency of LEO communications can be more than ten times lower than the one from Geostationary orbits. Furthermore, the smaller footprint of each antenna allows to reduce the size of the hardware components and, consequently, of the thruster, thus reducing the manufacturing costs of each satellite. Nevertheless, cheaper satellites are typically characterised by a shorter life-time cycle and, because the worst downside of LEO constellations rests in the number of satellites needed for (near) global coverage, this feature would also increase satellite traffic in LEO.

Constellation satellites have to be replaced once they reach their End-of-Life (EoL). Considering an average operational phase of 5 years as done in Radtke et al. (2017), more than 10 replacements per day would be necessary for the 18,348 already approved constellation's satellites considered in the current work. Furthermore, this will generate a two-way traffic, since a replacement involves the disposal of the EoL satellite and the injection of the new one.

According to the Union of Concerned Scientists satellite database (UCS, 2022) updated on January 1st 2022, there are currently 4,852 active satellites orbiting around Earth, 4,078 of which are in LEO. To these must be added around 3,000 satellites that are either dead or currently on their de-orbiting phase and more than 25,000 objects classified as space debris. In this environment, the injection of more than 18,000 satellites in LEO has already been approved, mostly by the FCC (Polli, 2021).

The increasing number of objects orbiting around Earth has motivated different analyses of the environmental impact of satellite constellations, mostly based on the interaction with space debris. In 1998, Rossi et al. (1998) developed a semi-deterministic model for the estimation of the number of collisions between satellite constellations and space debris based on a series of Monte Carlo (MC) simulations, also considering different traffic scenarios. In Rossi et al. (2017), the environmental impact of satellite constellations was analysed by mean of the Criticality of Constellation Index, or CCI. Different physical properties of the satellites, operational capabilities and constellation designs were considered for the 68 MC simulations performed. It was found that, among the investigated ones, the most critical parameters are: mass, area, and failure probability during the operational phase.

Other investigations rely on the ESA-MASTER software for the evaluation of the debris flux during the different phases of a constellation life cycle. The debris flux on the large constellations which most probably will be completed first, namely Starlink and OneWeb, was analysed accurately in Radtke et al. (2017) and Le May et al. (2018). As an example, considering

Business-As-Usual scenario, the probability of a catastrophic collision over the five years operational phase between a non-trackable debris and the high-altitude shells of the Starlink constellation evaluated in Le May et al. (2018) is 10.20 %.

The general approach for this type of risk assessments involves the characterization of the space debris environment in which the constellation is deployed, typically through a subdivision into volume elements. The collision probability is obtained from the number of collisions, which are statistically estimated. More precise algorithms can be used to assess the probability of a collision between two approaching objects, whose nominal orbits and position errors are known. Most known algorithms are Chan (2008), Alfano (2002), Foster & Estes (1992) and Patera (2000). More recent ones, such as Serra et al. (2016) and García-Pelayo & Hernando-Ayuso (2016), include analytical solutions in case of anisotropic distributions. All these methods are based on a three-dimensional Gaussian distribution of the satellites' positions and the collision probability is evaluated as the integral of the probability density function (PDF).

The objective of this study is to develop an analytical model that combines the efficiency of a statistical approach with the precision of a collision probability algorithm, in order to evaluate the mean collision probability related to a shell-crossing event. This type of event involves the passage of a de-orbiting or injecting satellite, under continuous tangential thrust, which has to cross the thin region of space populated by constellation's satellites, in order to reach its target destination. Given the large satellite population, most collision probability algorithms require large computational efforts to assess the risk related to an orbit-raising or -decreasing manoeuvre. On the other hand, the statistical model hereby presented is an efficient tool for preliminary mission design involving continuous tangential thrust. Moreover, the same model can be used to assess the collision probability with space debris, offering an alternative to the number of estimated collisions, which is currently used in software such as ESA-MASTER. Finally, given the statistical nature of the approach, this could represent a useful tool to assess the criticality of satellite injection and disposal, in a specific space environment. The model would be particularly convenient in this context, as it offers a risk assessment which does not depend on the position uncertainties of the satellites.

The injection of satellites can be divided into low- and high-thrust orbit raising. For LEO satellites, electric propulsion is typically adopted. This results in a continuous tangential low-thrust (Pollard, 2000) such that the satellite reaches its final orbit through a spiraling trajectory, having its semi-major axis continuously increasing. On the other hand, LEO satellites disposal is mainly performed via perigee decrease (Pollard, 1998). This consists in lowering the perigee and letting the greater atmospheric drag of the lower altitudes slow down the satellite until re-entry. In this study, continuous tangential low-thrusting has been considered for both injection and disposal, as it also includes passive re-entry.

The mathematical description of the satellite constellation refers to the Walker constellation (Walker, 1984). This is a highly symmetrical design for satellite constellations since it involves a set of equally inclined, equally populated and equally

spaced in RAAN circular orbits, all having the same semi-major axis. This is the most widely adopted design for large constellations and, due to its high degree of symmetry, allows for great simplifications for the evaluation of the average collision probability.

The environmental impact of satellite constellations is investigated by means of two different analyses: satellite constellation replacement and consequences of an in-orbit catastrophic collision. The former involves the evaluation of the mean collision probability between EoL de-orbiting satellites and new injecting satellites with both space debris and lower-altitude constellations. The latter assesses the collision probability between the cloud of fragments generated by an in-orbit collision, and lower-altitude constellations.

The remainder of the manuscript is organised as follows. In Section 2 a new model for estimation of collision probability averaged over every possible true anomaly phase between crossing and constellations satellites is presented. A simplified propagation model is developed in Section 3. This can be used to assess, in a highly efficient way, the collision probability profile over the initial true anomaly phase between crossing and constellation's satellites, when both orbits are circular. Section 4 presents the validation of both the statistical and the simplified propagation model. Constellations replacements and consequences of a in-orbit catastrophic collision are analysed, respectively, in Sections 5 and 6, using the statistical model developed in Section 2. Section 7 presents the conclusion.

2. Model

This section proposes a simplified statistical model specifically designed for the evaluation of the collision probability between a crossing satellite and all the satellites of a constellation shell, assuming every orbit to be circular.

The model is based on the assumption that all the \bar{N}_{CA} close approaches between the crossing satellite and one constellation's satellite, share the same probability \bar{P} that a collision will occur. Under this assumption, and considering the probabilities of different close approaches as independent, the overall collision probability $P_{satellite}$ between a constellation's and a crossing satellite is:

$$P_{satellite} = 1 - (1 - \bar{P})^{\bar{N}_{CA}} \quad (1)$$

In the following, the technique for the evaluation of \bar{P} and \bar{N}_{CA} will be explained.

2.1. Collision probability

In this section are presented the key ideas and the implementation of Chan's algorithm, for the evaluation of the collision probability between two orbiting objects. The formula obtained is then simplified by considering the orbits of both objects to be circular.

Let S_1 and S_2 be two satellites on their respective nominal orbits κ_1 and κ_2 , with covariance matrices at the time of closest

approach (TCA) ζ_1 and ζ_2 . Then, the collision probability between these two satellites can be evaluated using Chan's algorithm (Chan, 2008).

Let $[\mathbf{r}_1^N, \mathbf{v}_1^N]$ and $[\mathbf{r}_2^N, \mathbf{v}_2^N]$ be the Cartesian coordinates in the Earth-Centred Inertial (ECI) frame at the TCA of S_1 and S_2 , respectively. Then, the axes of the encounter reference frame Π centred at S_2 are defined at the TCA as follows:

- x -axis along the relative position vector $\Delta \mathbf{r}^N = \mathbf{r}_1^N - \mathbf{r}_2^N$
- y -axis along the relative velocity vector $\Delta \mathbf{v}^N = \mathbf{v}_1^N - \mathbf{v}_2^N$
- z -axis completing the set of principal axes

Note that x and y axes are perpendicular at TCA, as the miss distance $|\Delta \mathbf{r}^N|$ is minimum if and only if $\Delta \mathbf{r}^N \perp \Delta \mathbf{v}^N$. Moreover, recalling that the encounter plane is perpendicular to the relative velocity vector, this is the x - z plane.

The position of S_1 in Π is expressed as $\mathbf{r}_p = (d, 0, 0)$, where d is the nominal miss distance at the TCA. Modelling the satellites as spheres of radii R_1 and R_2 , the collision occurs when the relative distance between S_1 and S_2 is smaller than the radius of the combined hard sphere of the bodies, i.e. $r_a = R_1 + R_2$.

Under the hypothesis of uncorrelated measurements, the combined covariance matrix of the satellites can be computed as $\zeta = \zeta_1 + \zeta_2$ and it can be expressed as:

$$\zeta = \begin{bmatrix} \sigma_x^2 & \rho_{xy}\sigma_x\sigma_y & \rho_{xz}\sigma_x\sigma_z \\ \rho_{xy}\sigma_x\sigma_y & \sigma_y^2 & \rho_{yz}\sigma_y\sigma_z \\ \rho_{xz}\sigma_x\sigma_z & \rho_{yz}\sigma_y\sigma_z & \sigma_z^2 \end{bmatrix} \quad (2)$$

The PDF of a collision is modeled inside the x - z encounter plane. Moreover, the diagonal form of ζ' of the combined covariance matrix ζ can be obtained by moving through principal axes through a rotation around the y -axis. The required rotation angle γ is given by:

$$\gamma = \frac{1}{2} \tan^{-1} \left(\frac{2\rho_{xz}\sigma_x\sigma_z}{\sigma_x^2 - \sigma_z^2} \right) \quad (3)$$

and, on the encounter plane, it would be equal to:

$$\zeta' = \mathbf{R}_\gamma \cdot \zeta \cdot \mathbf{R}_\gamma^T = \begin{bmatrix} \sigma_{x'}^2 & 0 \\ 0 & \sigma_{z'}^2 \end{bmatrix} \quad (4)$$

where \mathbf{R}_γ is the rotation matrix of angle γ , around the y -axis. The collision probability P between S_1 and S_2 can be evaluated as (Chan, 2008):

$$P = e^{-\frac{V}{2}} \sum_{j=0}^{\infty} \frac{V^j}{2^j j!} \left[1 - e^{-\frac{U}{2}} \sum_{k=0}^j \frac{U^k}{2^k k!} \right] \quad (5)$$

where:

$$U = \left(\frac{r_a^2}{\sigma_{x'}\sigma_{z'}} \right) \quad V = \left(\frac{r_p'}{\sigma_{z'}} \right)^2 \quad (6)$$

Let r_p' be the miss distance vector in the encounter frame, then r_p'' is obtained by scaling r_p' along the x direction, such that the constant PDF ellipses turn into circles and the distribution becomes isotropic. It follows that:

$$r_p''^2 = \left(\frac{\sigma_{z'}}{\sigma_{x'}} d \cos \gamma \right)^2 + (d \sin \gamma)^2 \quad (7)$$

In Chan (2008) it is stated that, based on empirical evidences, the axes of a satellite error ellipsoid are almost aligned with the axes of its RSW reference frame. It follows that the covariance matrix of a satellite is almost diagonal in its RSW frame, this being defined as:

- R -axis along the radial direction, pointing towards the centre of Earth
- S -axis along the along-track direction, parallel to the velocity vector for circular orbits
- W -axis along the cross-track direction, completing the set of axes

If the covariance matrices ζ_1^{RSW} and ζ_2^{RSW} of, respectively, S_1 and S_2 are considered to be diagonal in their respective RSW reference frames (Chan, 2008), a great simplification of the problem is presented in Bai et al. (2013). The following encounter frame Π° is first defined:

- \hat{x} -axis along the radial direction of S_2
- \hat{y} -axis along the relative velocity between S_1 and S_2
- \hat{z} -axis completing the set of principal axes

The position of S_1 in Π° becomes:

$$\mathbf{r}_1^\circ = [\mu_{\hat{x}}, 0, \mu_{\hat{z}}] \quad (8)$$

where $d = \sqrt{\mu_{\hat{x}}^2 + \mu_{\hat{z}}^2}$ is the nominal miss distance at the TCA.

Let ζ_1^{RSW} and ζ_2^{RSW} be defined as:

$$\zeta_1^{RSW} = \begin{bmatrix} \sigma_{1R}^2 & 0 & 0 \\ 0 & \sigma_{1S}^2 & 0 \\ 0 & 0 & \sigma_{1W}^2 \end{bmatrix} \quad \zeta_2^{RSW} = \begin{bmatrix} \sigma_{2R}^2 & 0 & 0 \\ 0 & \sigma_{2S}^2 & 0 \\ 0 & 0 & \sigma_{2W}^2 \end{bmatrix} \quad (9)$$

then, the resulting combined covariance matrix ζ° on the encounter plane becomes:

$$\zeta^\circ = \begin{bmatrix} \sigma_{\hat{x}}^2 & 0 \\ 0 & \sigma_{\hat{z}}^2 \end{bmatrix} \quad (10)$$

where:

$$\sigma_{\hat{x}}^2 = \sigma_{1R}^2 + \sigma_{2R}^2 \quad (11a)$$

$$\sigma_{\hat{z}}^2 = (\sigma_{1S}^2 + \sigma_{2S}^2) \cos^2\left(\frac{\varphi}{2}\right) + (\sigma_{1W}^2 + \sigma_{2W}^2) \sin^2\left(\frac{\varphi}{2}\right) \quad (11b)$$

The angle φ is the angle between the angular momenta of the orbits κ_1 and κ_2 .

The collision probability can finally be evaluated as:

$$P = e^{-\frac{\hat{V}}{2}} \sum_{j=0}^{\infty} \frac{\hat{V}^j}{2^j j!} \left[1 - e^{-\frac{\hat{U}}{2}} \sum_{k=0}^j \frac{\hat{U}^k}{2^k k!} \right] \quad (12)$$

where:

$$\hat{U} = \left(\frac{r_a^2}{\sigma_{\hat{x}}^2 \sigma_{\hat{z}}^2} \right) \quad \hat{V} = \left(\frac{\mu_{\hat{x}}^2}{\sigma_{\hat{x}}^2} + \frac{\mu_{\hat{z}}^2}{\sigma_{\hat{z}}^2} \right) \quad (13)$$

Until now, three approximations have been introduced into the model:

- satellites are modeled as spheres
- PDF is modified to be isotropic
- error ellipsoids are aligned with RSW axes

For typical space applications, the errors arising from these simplifications are, in general, negligible.

2.2. Satellite dynamics

During the injection and active disposal phases the thrust is assumed to be tangential to the trajectory. This method is called tangential thrusting and represents the in-plane optimal control law for semi-major axis variations (Huang et al., 2021). Considering both atmospheric drag and thruster propulsion, the dynamics of the re-entering or newly deployed constellation's satellite are fully described through the expression of the semi-major axis variation:

$$\dot{a} = \dot{a}_{drag} + \dot{a}_{thrust} \quad (14)$$

where \dot{a}_{drag} and \dot{a}_{thrust} represent the semi-major axis rate of change due to air drag and tangential low-thrust, respectively. Using the Gauss form of the variational equation of semi-major axis reported in Battin (1999), the dynamics of a satellite on a circular orbit can be defined as:

$$\dot{a} = 2 \sqrt{\frac{a^3}{\mu}} a_\theta \quad (15)$$

where:

- a is the semi-major axis
- μ is Earth standard gravitational parameter
- a_θ is the transversal component of the perturbative acceleration vector \mathbf{a}_p

If Earth rotation is neglected, drag is always tangential to the satellite velocity and both forces act along the same direction. Nonetheless, the rotation of the atmosphere can still be considered for the estimation of \dot{a}_{drag} as follows:

$$\dot{a}_{drag} = -\sqrt{\mu a} \frac{\rho C_D A}{M} \left(1 - \frac{w_\oplus \cos i}{n} \right)^2 \quad (16)$$

where:

- ρ is the air density
- C_D is the drag coefficient
- A is the cross-sectional area of the spacecraft
- M is the mass of the spacecraft
- $w_\oplus = \frac{2\pi}{\text{day}}$ is the atmosphere angular velocity
- i is the inclination of the the orbit
- $n = \sqrt{\frac{\mu}{a^3}}$ is the mean motion of the spacecraft

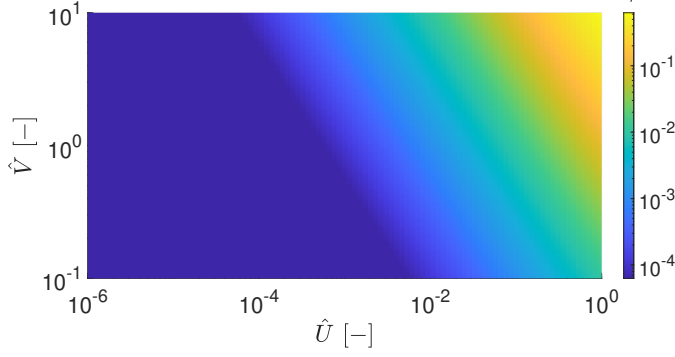


Fig. 1. Relative error ε_r between the 4th term and 1st term truncation of Eq. (12) for different values of \hat{U} and \hat{V} .

It must be emphasised that drag acceleration, in general, is not tangential to the satellite trajectory, due to the rotation of the atmosphere. Nevertheless, given the slow rate at which Earth rotates, these effects are considered to be negligible. The dynamics of the thruster are described as:

$$\dot{a}_{thrust} = \pm 4 \sqrt{\frac{a^3}{\mu} \frac{\eta_t P_t}{M g_0 I_{sp}}} \quad (17)$$

where:

- η_t is the efficiency of the thruster
- P_t is the input power of the thruster
- g_0 is the standard gravity
- I_{sp} is the specific impulse of the thruster

The derivation of Eq.s (16) and (17) are shown in Polli (2021) and Huang et al. (2021).

2.3. Collision probability distribution

The major benefit of Eq.s (5) and (12) is that the series converges rapidly (Chan, 2008). For typical satellites applications, it can be assumed that $\hat{U} < 10^{-4}$ and, as shown in Fig. 1, the truncation of Eq. (12) at the first term still yields accurate results.

The truncation at the first term of Eq. (12) is expressed through the following bivariate distribution:

$$P(\mu_{\hat{x}}, \mu_{\hat{z}}) = P_{\odot} \exp\left(-\frac{1}{2} \frac{\mu_{\hat{x}}^2}{\sigma_{\hat{x}}^2}\right) \exp\left(-\frac{1}{2} \frac{\mu_{\hat{z}}^2}{\sigma_{\hat{z}}^2}\right) \quad (18)$$

where:

$$P_{\odot} = 1 - \exp\left(-\frac{r_a^2}{2\sigma_{\hat{x}}\sigma_{\hat{z}}}\right) \quad (19)$$

does not depend on the miss distance, but rather on the geometrical and orbital properties of the satellites. P_{\odot} is the value of the maximum collision probability between two approaching satellites, which does occur when the nominal miss distance is null.

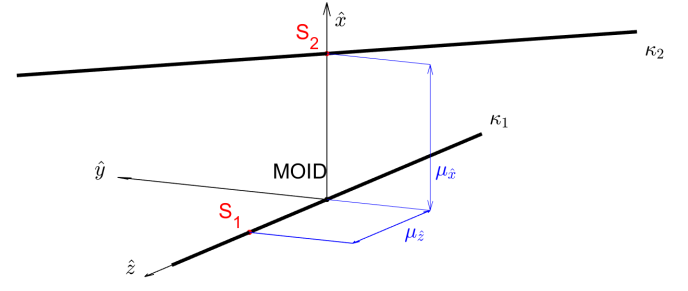


Fig. 2. Miss distance components in Π° reference frame when S_2 is at the MOID.

2.4. Nominal closest approach

In Bai et al. (2013), recalling Eq. (8), the miss distance vector at the TCA is defined on the encounter plane with the two components $\mu_{\hat{x}}$ and $\mu_{\hat{z}}$, where:

- $\mu_{\hat{x}}$ is the radial distance between S_1 and S_2
- $\mu_{\hat{z}}$ is the distance between S_1 and S_2 on the plane perpendicular to the radial direction

Let us consider S_1 to be a constellation satellite and S_2 a de-orbiting or injecting satellite, and let a_1 and a_2 be their respective semi-major axes. At the time instant in which S_2 is at the Minimum Orbit Intersection Distance (Gronchi, 2005), also known as MOID, depicted in Fig. 2, these two criteria are satisfied if:

$$\mu_{\hat{x}}^{\otimes} = \delta a \quad (20a)$$

$$\mu_{\hat{z}}^{\otimes} = \delta \omega a_1 \quad (20b)$$

where superscript \otimes denotes MOID, and:

- $\delta a = a_2 - a_1$ is the radial distance between S_1 and S_2
- $\delta \omega = \omega_2 - \omega_1$ is the angular phase between S_1 and S_2

True anomaly phase between satellites is defined using the arguments of periapsis ω , as only circular orbits are considered. Because S_1 and S_2 move along circular orbits, only values of δa in the order of a few kilometers typically lead to appreciable levels of collision probabilities. Therefore, a_1 and a_2 are in general very close and S_1 and S_2 can be considered to have equal velocity v . Moreover, for most cases, the MOID is close to the location of the NCA and the trajectories of both satellites in this interval can be considered to be linear. Under these hypotheses, the along-track distance $\mu_z(t)$ at the general time instant t can be computed (Polli, 2021) with respect to the along-track distance $\mu_z(t_0)$ at the time instant t_0 at which S_2 is at the MOID:

$$\mu_z^2(t) = \mu_z^2(t_0) + (2v^2 t^2 - 2\mu_z^2(t_0)vt)(1 - \cos \varphi) \quad (21)$$

Recalling that $\mu_{\hat{x}}$ is constant, the minimum miss distance corresponds to a minimum of $\mu_z^2(t)$. Imposing the derivative of Eq. (21) equal to zero, the miss distance vector at TCA is:

$$\mu_{\hat{x}} = \delta a \quad (22a)$$

$$\mu_{\hat{z}} = \delta \omega a_1 \cos \frac{\varphi}{2} \quad (22b)$$

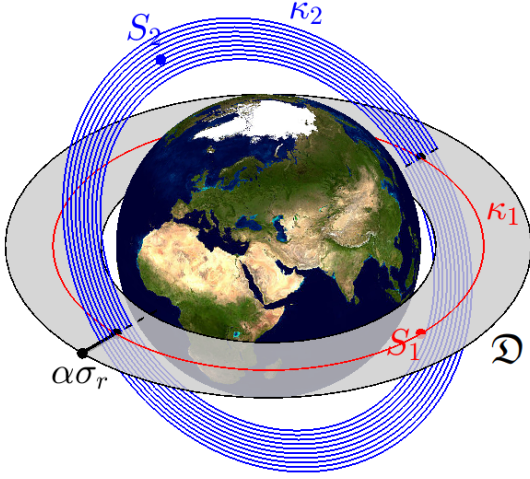


Fig. 3. shell-crossing event.

As a final remark, two circular orbits always share two MOIDs which are characterised by equal and opposite nominal miss distance vectors in ECI coordinates. Moreover, these vectors lie on the same line which also intersects Earth's centre.

2.5. Average collision probability with one constellation's satellite

The dynamics of a shell-crossing event are modeled such that the constellation satellite S_1 is on a fixed circular orbit, and the spiraling trajectory of the crossing satellite S_2 , which is eventually broken down into a series of a circular orbits, would result in a series of close approaches. This is represented in Fig. 3. For each revolution of S_2 , a maximum of two close approaches may occur. The overall collision probability can be evaluated by considering all together the collision probabilities related to each close approach.

Referring to Fig. 3, let us consider the annulus \mathfrak{D} centred at κ_1 of width $2\alpha\sigma_r$, where α is a parameter, to be the shell-crossing event domain. Then the mean collision probability \bar{P} over the domain \mathfrak{D} can be evaluated as:

$$\bar{P} = \frac{1}{\mathfrak{D}} \int_{\mathfrak{D}} P_{\odot} \exp\left(-\frac{1}{2} \frac{\mu_x^2}{\sigma_x^2}\right) \exp\left(-\frac{1}{2} \frac{\mu_z^2}{\sigma_z^2}\right) d\mu_x d\mu_z \quad (23)$$

Substituting Eq.s (22a) and (22b) into Eq. (23) and introducing the new variable $\delta z = a_1 \delta \omega$ yields:

$$\bar{P} = \frac{P_{\odot}}{\mathfrak{D}} \int_{\mathfrak{D}} \exp\left(-\frac{1}{2} \frac{\delta a^2}{\sigma_r^2}\right) \exp\left(-\frac{1}{2} \frac{\delta z^2}{\sigma_z^2}\right) d(\delta a) d(\delta z) \quad (24)$$

where:

$$\sigma_r^2 = \sigma_{\hat{x}}^2 = \sigma_{1r}^2 + \sigma_{2r}^2 \quad (25a)$$

$$\sigma_{\theta}^2 = \frac{\sigma_z^2}{\cos^2 \frac{\varphi}{2}} = (\sigma_{1s}^2 + \sigma_{2s}^2) + (\sigma_{1w}^2 + \sigma_{2w}^2) \tan^2 \frac{\varphi}{2} \quad (25b)$$

The area of the annulus \mathfrak{D} is:

$$\mathfrak{D} = \pi(a_1 + \alpha\sigma_r)^2 - \pi(a_1 - \alpha\sigma_r)^2 = 4\pi a_1 \alpha \sigma_r \quad (26)$$

Therefore, Eq. (24) can be written as:

$$\begin{aligned} \bar{P} &= \frac{P_{\odot}}{4\pi a_1 \alpha \sigma_r} \int_{-\alpha\sigma_r}^{\alpha\sigma_r} \exp\left(-\frac{1}{2} \frac{\delta a^2}{\sigma_r^2}\right) d(\delta a) \int_{-\pi a_1}^{\pi a_1} \exp\left(-\frac{1}{2} \frac{\delta z^2}{\sigma_z^2}\right) d(\delta z) \\ &= \frac{1}{\alpha} \frac{P_{\odot}}{2} \frac{\sigma_{\theta}}{a_1} \operatorname{erf}\left(\frac{1}{\sqrt{2}} \alpha\right) \operatorname{erf}\left(\frac{1}{\sqrt{2}} \frac{\pi a_1}{\sigma_{\theta}}\right) \\ &\approx \frac{1}{\alpha} \frac{P_{\odot}}{2} \frac{\sigma_{\theta}}{a_1} \operatorname{erf}\left(\frac{1}{\sqrt{2}} \alpha\right) \end{aligned} \quad (27)$$

For typical satellite applications $a \gg \sigma_{\theta}$ and $\operatorname{erf}\left(\frac{1}{\sqrt{2}} \frac{\pi a_1}{\sigma_{\theta}}\right) \approx 1$.

Following the same reasoning, a close approach will occur if both S_1 and S_2 are within \mathfrak{D} at the same instant. As S_1 always lies on \mathfrak{D} , a close approach will occur when S_2 crosses the domain \mathfrak{D} , that is when S_2 is at the MOID. It follows that for every revolution of S_2 , two close approaches will occur and:

$$\bar{N}_{CA} = 2R_{\mathfrak{D}} \quad (28)$$

where $R_{\mathfrak{D}}$ is the number of revolutions of S_2 that intersect the domain \mathfrak{D} .

The number of revolutions $R_{\mathfrak{D}}$ is computed as the ratio between the width of the annulus \mathfrak{D} and the semi-major axis variation per revolution $|\Delta a|$ of S_2 , therefore Eq. (28) can be written as:

$$\bar{N}_{CA} = 4 \frac{\alpha \sigma_r}{|\Delta a|} \quad (29)$$

and the semi-major axis variation, which is assumed to be constant during the shell-crossing event, is:

$$\Delta a = \dot{a} T_1 \quad (30)$$

where T_1 is the orbital period of S_1 .

Finally, the mean collision probability $P_{\text{satellite}}$ between a crossing satellite and a constellation satellite can be obtained by imposing the domain \mathfrak{D} to have infinite radial extension, thus:

$$\begin{aligned} P_{\text{satellite}} &= \lim_{\alpha \rightarrow +\infty} \left\{ 1 - \left[1 - \frac{1}{\alpha} \frac{P_{\odot}}{2} \frac{\sigma_{\theta}}{a_1} \operatorname{erf}\left(\frac{\alpha}{\sqrt{2}}\right) \right]^4 \right\} \\ &= 1 - \exp\left(-2 \frac{P_{\odot} \sigma_r \sigma_{\theta}}{|\Delta a| a_1}\right) \end{aligned} \quad (31)$$

2.6. Head-on collisions

The hypothesis of linear motion of both satellites between MOID and NCA in Section 2.5, cannot be considered valid anymore in case of head-on collisions, as the collision PDF is not condensed in the vicinity of the MOID. That is when κ_1 and κ_2 are characterised by (almost) parallel angular momenta, but with opposite directions.

The time instants t_0 and t^* in Fig. 4, respectively refer to the time instant in which S_2 is at the MOID and the TCA. As before, assuming both the constellation's and crossing satellites to have equal angular velocity, the angle $\nu(t)$ represented in Fig. 4 can be expressed using the cosine rule as:

$$\cos \nu(t) = \cos(nt) \cos(\delta\omega - nt) + \sin(nt) \sin(\delta\omega - nt) \cos(\pi - \varphi) \quad (32)$$

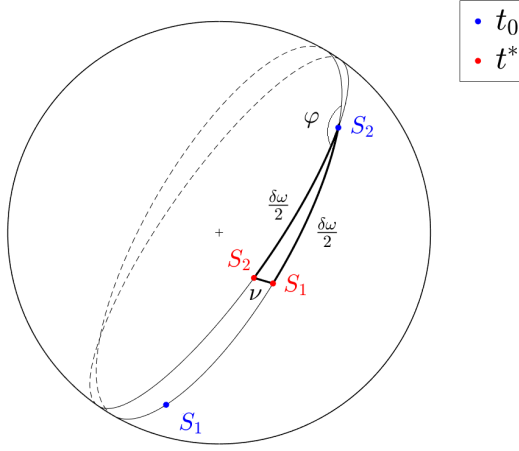


Fig. 4. Non-scaled representation of NCA for near straight collision angles φ .

Imposing the derivative of Eq. (32) equal to zero, as previously done in Section 2.4, and recalling that for head-on collisions $\mu_z = a_1 \nu$, yields:

$$\mu_z = 2a_1 \sin \frac{\delta\omega}{2} \cos \frac{\varphi}{2} \quad (33)$$

Finally, using the same method from Section 2.5 for the evaluation of \bar{P} and, again, considering the annular domain \mathfrak{D} to have infinite radial extension, the overall collision probability $P_{satellite}$ between one constellation's and one crossing satellite can be evaluated as:

$$P_{satellite} = 1 - \exp \left[-2 \sqrt{2\pi} \frac{P_{\odot} \sigma_r}{|\Delta a|} \exp \left(-\frac{a_1^2}{\sigma_{\theta}^2} \right) I_0 \left(\frac{a_1^2}{\sigma_{\theta}^2} \right) \right] \quad (34)$$

where I_0 is the modified Bessel function of the first kind of order zero.

2.7. Average collision probability of a shell-crossing event

In general, more than one satellite moves along the orbit κ_1 of a satellite constellation (Walker, 1984). Let N_S be the number of satellites on one constellation's orbital plane, as shown in Fig. 5.

The average collision probability P_{plane} with one constellation's orbital plane can be evaluated by using Eq.s (31) and (34) for each one of the N_S satellites. Nevertheless, the evaluation is simplified if all the N_S satellites are assumed to have equal error ellipsoid in their respective RSW reference frames. Indeed, under this hypothesis, the crossing satellite has the same average collision probability with each one of the N_S constellation's satellites belonging to a single orbital plane. Assuming the collision probabilities with each satellite to be independent from one another, then:

$$P_{plane} = 1 - (1 - P_{satellite})^{N_S} \quad (35)$$

Referring to the general case described in Section 2.5, P_{plane} can be computed as:

$$P_{plane} = 1 - \exp \left(-2 \frac{P_{\odot} N_S \sigma_r \sigma_{\theta}}{|\Delta a| a_1} \right) \quad (36)$$

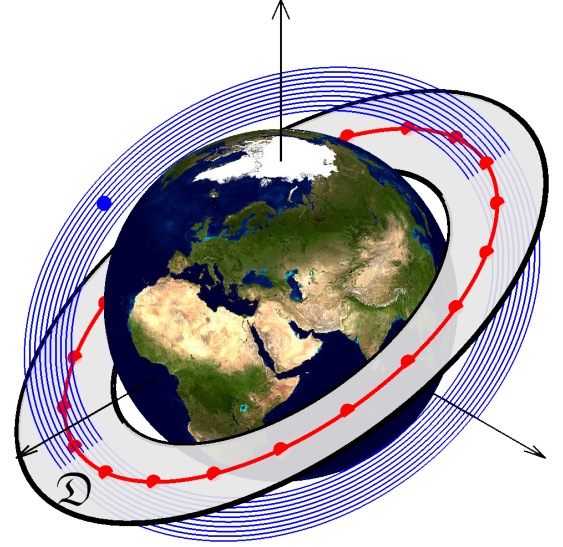


Fig. 5. One constellation's orbital plane with N_S satellites.

whereas for the head-on collision case from Section 2.6:

$$P_{plane} = 1 - \exp \left[-2 \sqrt{2\pi} \frac{P_{\odot} N_S \sigma_r}{|\Delta a|} \exp \left(-\frac{a_1^2}{\sigma_{\theta}^2} \right) I_0 \left(\frac{a_1^2}{\sigma_{\theta}^2} \right) \right] \quad (37)$$

Finally, the average collision probability P_{shell} related to a shell-crossing event can be computed as:

$$P_{shell} = 1 - \prod_{i=1}^{N_P} (1 - P_{plane,i}) \quad (38)$$

where N_P is the total number of orbital planes of the constellation.

2.8. Threshold collision angle

The expression of $P_{plane,i}$ in Eq. (38) depends on the angle φ_i between the crossing orbital plane and the i -th orbital plane of the constellation. It must be emphasised that Eq. (36) holds if $\varphi \neq \pi$, whereas Eq. (37) is always valid. Nonetheless, the expressions $\exp \left(-\frac{a_1^2}{\sigma_{\theta}^2} \right)$ and $I_0 \left(\frac{a_1^2}{\sigma_{\theta}^2} \right)$ exponentially decrease and increase, respectively, the smaller φ is. This would result in numerical values out of the floating-point range normally supported by most computational software.

It follows that a threshold value φ^* has to be defined to distinguish whether Eq. (36) or Eq. (37) has to be used. In this study, MATLAB is used for constellation risk assessments, which has a largest positive floating-point number of around 1.7×10^{308} (double precision). Let:

$$\Phi_{max} = \frac{a_1}{\sigma_{\theta}(\varphi^*)} \quad (39)$$

such that $I_0(\Phi_{max}^2) < N_{fp,max}$, where $N_{fp,max}$ is the largest floating-point number available.

Recalling equation 25b, the threshold angle φ^* can be computed as:

$$\varphi^* = 2 \tan^{-1} \sqrt{\frac{1}{\sigma_W^2} \left(\frac{a_1^2}{\Phi_{max}^2} - \sigma_S^2 \right)} \quad (40)$$

where:

$$\sigma_S^2 = \sigma_{1_S}^2 + \sigma_{2_S}^2 \quad (41a)$$

$$\sigma_W^2 = \sigma_{1_W}^2 + \sigma_{2_W}^2 \quad (41b)$$

In the following sections, a value of $\Phi_{max} = 12.5$ has been used. An alternative strategy involves the definition of a maximum relative error ε_Φ between Eq.s (36) and (37). The threshold angle φ^* can be then computed as:

$$\tan^2 \frac{\varphi^*}{2} \approx 8 \frac{a_1^2}{\sigma_W^2} \frac{\varepsilon_\Phi}{1 - \varepsilon_\Phi} \quad (42)$$

The continuity between Eq.s (36) and (37) in a neighborhood of φ^* can also be proven, as shown in Polli (2021). Moreover, if $\varphi_i \leq \varphi^*$ for all i , which means the absence of potential heads-on collisions, then, substituting Eq. (36) into Eq. (38), and considering its Maclaurin expansion:

$$P_{shell} \approx \frac{N_S r_a^2}{|\Delta a| a_1} \sum_{i=1}^{N_P} \frac{1}{\cos \frac{\varphi_i}{2}} \quad (43)$$

where P_{shell} does not depend anymore on the position uncertainties of the crossing and constellation's satellites.

2.9. Summary of hypotheses

The model developed in this section is based on the following assumptions:

1. All the effects of natural perturbations are neglected, with the only exception of altitude variation due to air drag
2. All satellites are assumed to move along circular orbits
3. The altitude drop per orbit of S_2 inside \mathfrak{D} is considered to be constant
4. The covariance matrices of the position error of both satellites are assumed to be diagonal in their respective RSW reference frames (Chan, 2008)
5. The satellites are modeled as spheres
6. The collision probabilities of each close approach are assumed to be independent from one another

3. MOID propagation model

The statistical model developed in Section 2 is an efficient tool for risk assessments of highly populated traffic scenarios. On the other hand, it fails to consider phase between satellites. For this purpose, the MOID propagation model has been developed.

This is a simplified propagation model whose time step is equal to half the orbital period of the constellation satellite. Each iteration is composed of three main steps:

- altitude variation of S_1
- phase shift between S_1 and S_2 due to different orbital periods
- collision probability assessment at NCA

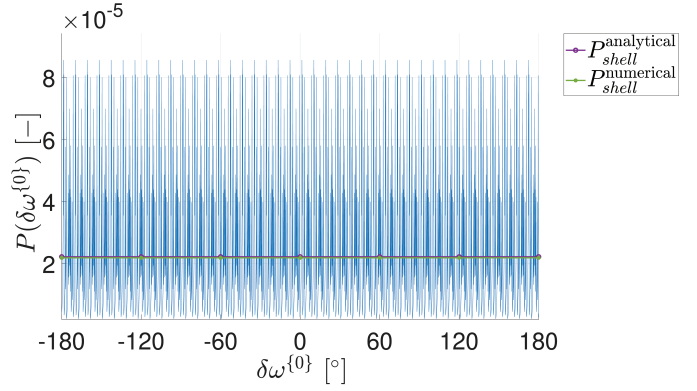


Fig. 6. Collision probability distribution $P(\delta\omega^{(0)})$ and its mean value P_{shell} of a satellite crossing OneWeb constellation with $|\Delta a| = 0.1$ km/s.

Significant values of collision probabilities require both objects to be relatively close to one another. Therefore, considering the orbits to be circular within the propagation time step, it follows that $a_1 \approx a_2$. With this consideration in mind, the semi-major axis of S_2 at each time step would be:

$$a_2^{[k+1]} = a_2^{[k]} + \frac{\Delta a}{2} \quad (44)$$

Following the same reasoning, S_1 true anomaly can be estimated as:

$$\theta^{[k+1]} = \theta^{[k]} + \pi \left(\frac{a_1}{a_2^{[k]}} \right)^{\frac{3}{2}} \quad (45)$$

Let the constellation satellite be at one of the two MOIDs at the initial propagation time $t = 0$, then at each step it will always be located, alternately, at the two MOIDs. Under this condition, the miss distance of every NCA can be computed with Eq.s (22a) and (22b), or Eq. (33) if $\varphi > \varphi^*$, where:

$$\delta a^{[k+1]} = \delta a^{[k]} + \frac{\Delta a}{2} \quad (46a)$$

$$\delta \omega^{[k+1]} = \delta \omega^{[k]} + \pi \left[1 - \left(\frac{a_1}{a_2^{[k]}} \right)^{\frac{3}{2}} \right] \quad (46b)$$

The overall collision probability $P(\delta\omega^{(0)})$ can be evaluated through the combination of the collision probabilities of each NCA, computed with Chan's algorithm truncated at the 4th term. Repeating the process for different initial true anomaly phases $\delta\omega^{(0)}$, the collision probability profile shown in Fig. 6 is obtained. The analytical evaluation of P_{shell} from Fig. (6) refers to Eq. (38), whereas its numerical value is given as the integral of the distribution obtained with the MOID propagation model. It has been extensively demonstrated that these two always correspond (Polli, 2021), hence, the following relation holds:

$$P_{shell} = 1 - \prod_{i=1}^{N_P} (1 - P_{plane,i}) \approx \frac{1}{2\pi} \int_0^{2\pi} P(\delta\omega^{(0)}) d(\delta\omega^{(0)}) \quad (47)$$

Eq. (47) has been validated for different constellations, $|\Delta a|$, σ_1^{RSW} , σ_2^{RSW} and orientations of the crossing orbital plane.

Nonetheless, it must be emphasised that Eq. (47) cannot be considered always valid, as large values of semi-major axis variation per revolution $|\Delta a|$, would result in a fewer number of close approaches. In this context, a statistical approach fails to be consistent within acceptable error boundaries, as the mean collision probability over the true anomaly phase also depends on the initial radial distance $\delta a^{(0)}$.

It has been observed that, recalling Eq. (25a), Eq. (47) holds with a relative error lower than 1×10^{-3} , if:

$$\frac{3\sigma_r}{|\Delta a|} \geq 1 \quad (48)$$

In Polli (2021) it is shown that, if Eq. (48) is not satisfied, the average collision probability over the true anomaly phase follows a sinusoidal-like behaviour which depends on $\delta a^{(0)}$, and has a period equal to $|\Delta a|$. Under this condition, the statistical model presented in Section 2 assesses the mean collision probability, which is averaged over both $\delta \omega^{(0)}$ and $\delta a^{(0)}$.

A series of MC simulations using different values of $\mu_{\hat{x}}$ and $\mu_{\hat{z}}$ have also been performed in order to validate the assumption of using Chan's algorithm truncated at the first term (Polli, 2021). From Fig. 6 is clear how the true anomaly phase $\delta \omega$ plays a key role for collision probability minimisation. The MOID propagation model also constitutes an efficient tool for collision probability assessments, as the collision probability spectrum over the true anomaly phase can be outlined with extremely low computational effort.

Indeed, the larger the semi-major axis rate of change $|\Delta a|$, the more efficient the MOID propagation model, since fewer close approaches have to be assessed. Conveniently, that is the case in which a statistical approach loses its validity.

4. Validation

Most of the assumptions on which the statistical model is based, listed in Section 2.9, do not considerably change the dynamics of the shell-crossing event. The most stringent hypotheses are the first two: neglecting other natural sources of perturbation (J_2 in particular) and discretising the spiraling trajectory of the crossing satellite into circular orbits. In this section, the validity of the latter is assessed, for different values of eccentricity of the crossing orbit.

The most suitable option for validation would be a series of MC simulations for different values of initial phase $\delta \omega^{(0)}$. Then, the average collision probability could be computed with Eq. (47). Nevertheless, billions of MC runs would be necessary to analyse the collision probability profile over the initial phase $\delta \omega^{(0)}$, and this process would have to be repeated for different relative orientations between κ_1 and κ_2 , i. e. for different values of φ .

As this would require to much computational power, a different approach is hereby used. The motion of two satellites, one from the constellation and one crossing it, are propagated through the integration of the equations of motion in Cartesian coordinates. Once the nominal orbits are known, NCAs are detected and their respective collision probability is computed with Chan's

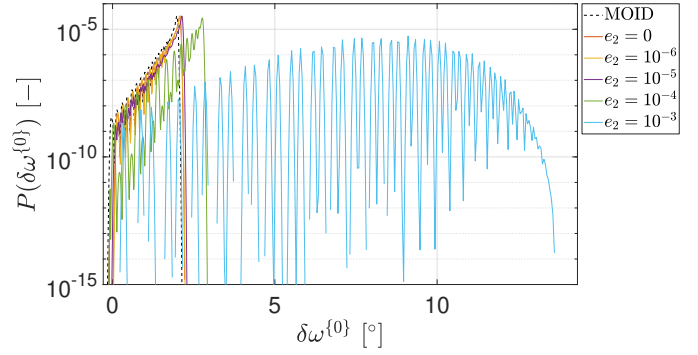


Fig. 7. Comparison between the collision probability profiles $P(\delta \omega^{(0)})$ obtained with the MOID propagation model, and standard propagation assuming different initial eccentricity of the crossing satellite. Simulation data: $\varphi = \frac{\pi}{6}$, $\zeta_1^{\text{RSW}} = \text{diag}\{1/4, 1, 1/4\}$ km², $\zeta_2^{\text{RSW}} = \text{diag}\{1, 4, 1\}$ km², $r_a = 4$, $C_D = 2.2$, $P_t = 400$ W, $\eta = 0.5$, $I_{sp} = 3000$ s.

algorithm truncated at the 4th term. The position uncertainties of the satellites are considered to be constant in their respective RSW frame, during the duration of the shell-crossing event.

It is worth mentioning that the error introduced by this last assumption may affects the results locally, but the overall effect on the average collision probability could be negligible. Further investigations about this topic are desirable, but limited by the great computational effort required.

In Fig. 7 is represented the collision probability spectrum $P(\delta \omega^{(0)})$ evaluated with both MOID and standard propagation models. The latter has been used for different values of initial orbit eccentricity e_2 . Simulations were carried out considering two Starlink satellites of mass 386 kg and cross-sectional radius of 2.39 m (Le May et al., 2018), both belonging to the Starlink (4) shell from Table 1. The crossing satellite is de-orbiting.

The collision probability profiles $P(\delta \omega^{(0)})$ were used to evaluate the average collision probabilities of the shell-crossing events, exploiting trapezoidal numerical integration. These results are listed in Table 2, from which it can be noticed that the statistical model is able to predict with great accuracy the collision probability for crossing orbit eccentricity up to 10^{-3} . It was not possible to test larger values of eccentricity due to the considerable computational effort required. Moreover, the larger e_2 , the less accurate is the result, as a wider interval of initial true anomaly phases $\delta \omega^{(0)}$ decreases the resolution of the collision probability profile $P(\delta \omega^{(0)})$.

Considering Fig. 7, a larger eccentricity e_2 affects the collision probability spectrum by spreading lower values of $P(\delta \omega^{(0)})$ over a wider range of $\delta \omega^{(0)}$, keeping its mean value constant. Hence, when crossing crowded constellations, the lower e_2 , the more the collision probability can be minimised through the proper selection of $\delta \omega^{(0)}$.

A final remark has to be made about gravitational perturbations due to Earth's oblateness, as it strongly affects the dynamics of low-altitude orbits. It was observed that the altitude variation caused by considering J_2 , decreases the probability per revolution that a close approach will occur, but increases the number of overall revolutions in the vicinity of the constellation's orbit κ_1 . Further analyses may be the subject for future studies.

Table 1. Catalogue of the satellite constellations considered in the study.

Constellation	i_1 [°]	N_T	N_P	f	h [km]	Shell	Status ^a	Reference
Starlink	42	2493	42	2	336	(1)	A	FCC (2018-2021)
	48	2478	42	2	341	(2)	A	
	53	2547	42	2	346	(3)	A	
	53.2	1584	72	2	540	(4)	A	
	53	1584	72	2	550	(5)	D	
	97.6	348	6	2	560	(6)	A	
	97.6	172	4	2	565	(7)	A	
	70	720	36	2	570	(8)	A	
Kuiper	33	784	28	2	590	(1)	A	FCC (2019)
	42	1296	36	2	610	(2)	A	
	51.9	1156	34	2	630	(3)	A	
Telesat	98.98	351	27	3	1015	(1)	C	FCC (2020b)
	50.88	1320	33	3	1320	(2)	A	
OneWeb	87.9	720	18	2	1200	-	D	FCC (2020a)
Kepler	89.5	360	12	2	600	-	A	
Iridium NEXT	86.4	66	6	2	770	-	C	FCC (2016)
Globalstar	52	48	8	2	1414	-	C	FCC (2011)
OrbcommG1	45	12	3	3	775	(1)	C	FCC (2008)
	108	2	1	1	780	(2)	C	
	70	2	1	1	785	(3)	C	
	45	24	3	3	820	(4)	C	
	0	8	1	1	825	(5)	C	
Capella Space	98	36	12	2	495	-	D	Kramer (2019)
Swarm Tech	45	20	1	1	450	(1)	C	FCC (2018)
	10	20	1	1	500	(2)	C	
	97.4	62	1	1	505	(3)	C	
	97.6	48	1	1	555	(4)	C	
Planet	51.6	28	1	1	410	(1)	C	FCC (2013)
	51.6	28	1	1	415	(2)	C	
	97.98	11	1	1	620	(3)	C	
HawkEye 360	14.25	2	1	1	575	(1)	C	FCC (2017)
	45	10	5	5	580	(2)	C	
	14.25	2	1	1	585	(3)	C	

^a(A) Approved (D) Deployment (C) CompletedTable 2. Shell-crossing event average collision probability evaluated with Cartesian propagation and Chan's algorithm for different initial crossing eccentricity e_2 and collision angle φ . Respective values of P_{shell} are reported for comparison.

e_2 [-] \ φ [rad]	$\frac{\pi}{6}$	$\frac{\pi}{3}$	$\frac{\pi}{2}$	$\frac{2\pi}{3}$	$\frac{5\pi}{6}$	π
0	0.91218×10^{-8}	0.10177×10^{-7}	0.12469×10^{-7}	0.17638×10^{-7}	0.34075×10^{-7}	0.13678×10^{-3}
10^{-6}	0.91246×10^{-8}	0.10179×10^{-7}	0.12470×10^{-7}	0.17638×10^{-7}	0.34075×10^{-7}	0.13678×10^{-3}
10^{-5}	0.91423×10^{-8}	0.11019×10^{-7}	0.12477×10^{-7}	0.17639×10^{-7}	0.34076×10^{-7}	0.13679×10^{-3}
10^{-4}	0.91404×10^{-8}	0.10192×10^{-7}	0.12477×10^{-7}	0.17640×10^{-7}	0.34078×10^{-7}	0.13678×10^{-3}
10^{-3}	0.90144×10^{-8}	0.10077×10^{-7}	0.12393×10^{-7}	0.17614×10^{-7}	0.34076×10^{-7}	0.13673×10^{-3}
P_{shell}	0.91313×10^{-8}	0.10185×10^{-7}	0.12474×10^{-7}	0.17640×10^{-7}	0.34078×10^{-7}	0.13680×10^{-3}

5. Constellation's replacement risk assessment

The statistical model developed in Section 2 will be used in this section to appraise the environmental hazard of satellite constellations. In particular, a risk assessment analysis of the disposal and injection phases of satellite constellations will be performed, also considering the presence of space debris and different Post-Mission Disposal (PMD) success rates.

The constellations considered are summarised in Table 1 and they are all modeled as Walker constellations, which are fully described by the inclination i_1 , the total number of satellites N_T , the number of orbital planes N_P , the relative phase shift between satellites on adjacent planes f and the altitude of the shell h . Most of these constellations were approved by the FCC, the authority regulating telecommunications in the United States.

The current section investigates, from a collision probability standpoint, the environmental consequences of the increase in LEO traffic that would result from constellation's satellites that have to be replaced, once they have reached their EoL.

5.1. Optimal crossing

The structure of a satellite constellation is considered to be fixed in time, thus the inclination i_1 and RAAN Ω_1 of each orbital plane are constant. The relative orientation between constellation's and crossing satellites, hence, depends on the inclination and RAAN of the crossing satellite.

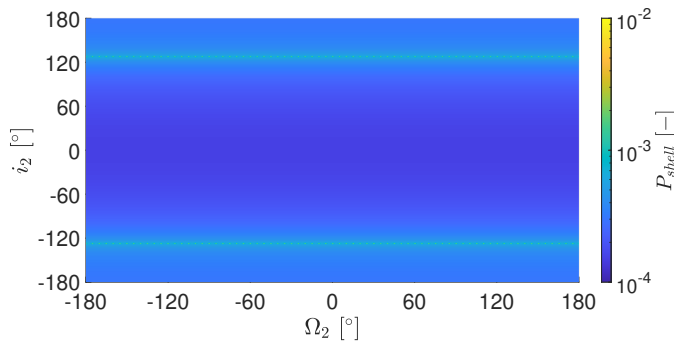


Fig. 8. Collision probability distribution of passive de-orbiting through Starlink (4) shell.

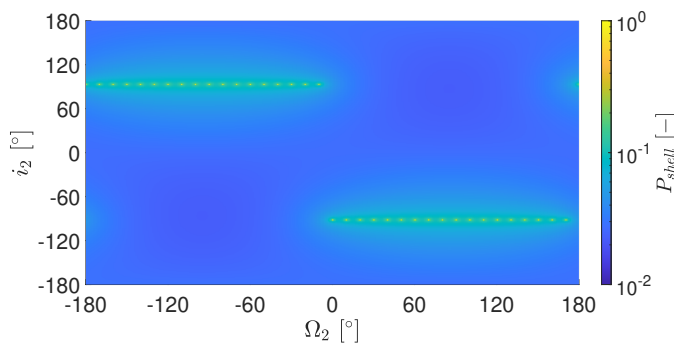


Fig. 9. Collision probability distribution of passive de-orbiting through OneWeb shell.

In Figs 8 and 9 are represented the collision probability distributions related to, respectively, a Starlink (4) and OneWeb shell-crossing event, for different inclinations i_2 and RAANs Ω_2 of the crossing satellite. Each peak in Figs 8 and 9 corresponds to the case of head-on collision with one of the orbital planes of the constellation. It can also be noticed that the minimum mean collision probability P_{shell} occurs when $i_2 = 0^\circ$.

To better understand this last statement, consider the collision angle distributions between a crossing satellite and a Starlink (4) and OneWeb orbital plane, respectively shown in Figs 10 and 11.

The collision angle φ between κ_1 and κ_2 can be computed as:

$$\cos \varphi = \sin i_1 \sin i_2 \cos \Delta \Omega + \cos i_1 \cos i_2 \quad (49)$$

Because i_1 and i_2 are constant, the distribution of collision angles φ_i between the crossing orbital plane and the various constellation's orbital planes depends on $\cos(\Delta \Omega_i)$. As the constellation's orbital planes are equally spaced in RAAN, the collision angles characterising a shell-crossing event follow a cosinusoidal-like behaviour, whose mean value $\bar{\varphi}$ can be computed as:

$$\cos(\bar{\varphi}) = \cos i_1 \cos i_2 \quad (50)$$

Imposing the derivative of Eq. (50) over i_2 equal to zero, returns the condition for which $\bar{\varphi}$ is either maximum or minimum. That is when i_2 is either null or straight. In particular, $\bar{\varphi}$ is minimum

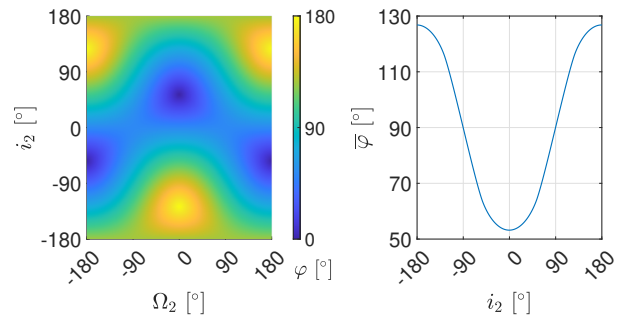


Fig. 10. Distribution of the collision angle φ between one orbital plane of Starlink (4) and any possible crossing orbital plane (left) and its mean value over the RAAN $\bar{\varphi}$ (right).

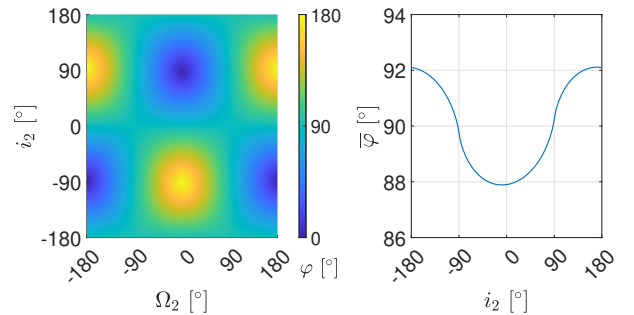


Fig. 11. Distribution of the collision angle φ between one orbital plane of OneWeb and any possible crossing orbital plane (left) and its mean value over the RAAN $\bar{\varphi}$ (right).

Table 3. Data used in Section 5.

	Value	Symbol
S_1 covariance	$\text{diag}\{0.25, 1, 0.25\} \text{ km}^2$	ξ_1^{RSW}
S_2 covariance	$\text{diag}\{1, 4, 1\} \text{ km}^2$	ξ_2^{RSW}
Drag coefficient	2.2	C_D
Input power	600 W	P_t
Thruster efficiency	0.5	η_t
Specific impulse	2000 s	I_{sp}
Maximum $\frac{a_1}{\sigma_\theta}$ ratio	12.5	Φ_{max}

if the crossing orbital plane has inclination i_2 such that:

$$i_2 = 0^\circ \quad \text{if } \cos i_1 \geq 0 \quad (51a)$$

$$i_2 = 180^\circ \quad \text{if } \cos i_1 \leq 0 \quad (51b)$$

Substituting Eq.s (51a) and (51b) into Eq. (49), one obtains that $\cos \varphi$ is constant for all i , and always greater than zero. This is a rather important condition for collision probability minimisation, as the collision angles are guaranteed to be lower than (or equal to) 90° .

Up to this point, one could argue that the results obtained in Eq. (51) minimise the average collision angle $\bar{\varphi}$, but not necessarily the collision probability of the shell-crossing event P_{shell} . Nonetheless, P_{shell} is characterised by a super-linear dependence on φ , meaning that, the larger the amplitude of the distribution of collision angles φ_i , the larger the overall collision probability P_{shell} . The conditions expressed in Eq. (51) guarantee a constant distribution of collision angles φ_i with minimum mean value, thus minimising P_{shell} .

Considering that the inclinations in Table 1 are, for the most part, lower than 90° . then, the equatorial plane would be the optimal gateway orbital plane for both satellite injection and disposal for collision probability minimisation. A side advantage of the optimal crossing orbit is that it has the optimal inclination needed in order to fully exploit Earth rotation during launch, hence reducing costs.

It must be highlighted that the result obtained for optimal crossing is limited to constellations whose orbital planes have RAAN spanning over 360° . Indeed, this is not the case for constellations characterised by polar orbits, for which RAAN interval is typically less than 180° . This feature allows for shell-crossing events with collision angles always smaller than (or equal to) $\bar{\varphi}$, as defined in Eq. (50).

Consider the 18 orbital planes of OneWeb constellation to have equally spaced RAANs between 0° and 170° and inclination $i_1 = 87.9^\circ$. Then, optimal crossing can be achieved with a crossing orbital plane having inclination i_2 equal to i_1 , and RAAN equal to 85° . Nonetheless, repeatedly changing the inclination of the crossing satellite from 0° to near-polar and vice versa is broadly inefficient. Moreover, crossing polar constellation through the equatorial plane leads to constant collision angles marginally lower than (or equal to) 90° , and, as it can be seen from Table 2, P_{shell} is less affected at low φ .

Finally, optimal crossing can, sometimes, be a poor choice in terms of fuel (or time) consumption. Furthermore, as the changes in P_{shell} are considerable only for large values of colli-

sion angles, trade-offs between collision probability minimisation and fuel consumption are, in general, recommended.

5.2. Methodology

The risk assessment is performed by considering the EoL satellite that has to de-orbit and the new satellite that shall replace it. For both satellites, space debris and constellations that have to be crossed are considered as collision sources and the overall collision probability is computed as a combination of these two. The collision probability with other constellations is assessed using the model developed in Section 2, whereas the ESA-MASTER software, as done in (Radtke et al., 2017) and Le May et al. (2018), is used for the evaluation of the collision probability with space debris (Polli, 2021).

Let P^\pm be the collision probabilities of the injecting and de-orbiting satellite, respectively; then:

$$P^\pm = 1 - (1 - P_c^\pm)(1 - P_d^\pm) \quad (52)$$

where P_c and P_d are the probabilities that a collision will occur, respectively, with constellations and debris.

The overall collision probability related to the full replacement of a shell, can finally be computed as:

$$P_{tot} = 1 - [(1 - P^+)(1 - P^-)]^{N_T} \quad (53)$$

The constellations are eventually divided into two categories, based on their scope: Telecommunication (T) or Earth-Observation (EO). Satellites belonging to either category are modeled as spheres, the former having an average radius of 2 m and mass of 200 kg, the latter of 0.5 m and 50 kg. The combined hard sphere radius r_a is given by the sum of the cross-sectional radii of constellation and crossing satellites. Table 3 collects data used for simulations.

5.3. Results

The collision probability of a full constellation replacement has been evaluated for every constellation considering different engine input powers and two different scenarios: best case scenario (**B**) corresponds to a crossing orbit having zero inclination, whereas, in nominal case scenario (**N**) the crossing orbital plane is assumed to be an orbital plane of the arrival or departure shell. It follows that the inclination of the crossing satellite will be $i_2 = i_1$. Results are shown in Figs 12 and 13.

Figs 14 and 15 show more details about the risk assessment related to the replacement of Kuiper (3) shell, considering optimal crossing only for injecting satellites. Recalling Section

5.2, in Fig. 14 are represented the collision probabilities P_c^\pm , P_d^\pm and P^\pm for different values of engine input power, and Fig. 15 shows how P_c^\pm are partitioned among the various shells.

Finally, by assuming that failed EoL satellites re-enter through passive de-orbiting, different PMD success rates can be considered for the risk assessment analysis. As the Starlink constellation is, by far, the most populated one, in Fig. 16 are shown the collision probabilities related to the full replacement of the Starlink constellation with different PMD success rates, considering both scenarios **B** and **N**. The vertical black line refers to a failure rate of 1.45×10^{-2} , which is the one currently declared by Starlink (Kramer, 2021).

As expected from the results collected in Table 2, Figs. 12 and 13 show that the improvement of scenario B over N, are not considerable. The benefits of optimal crossing can be appreciated in Fig. 16, where a large number of satellites is considered. The effects of the thruster acceleration on the collision probability can be observed in Figs. 12 and 13, where it is shown that increasing the propulsion of the satellite can reduce it by one order of magnitude at higher altitude.

Other parameters that affect replacement collision probability are size and number of constellation satellites. Due to their much smaller size, Earth observation satellites are characterised by impact probabilities several orders of magnitude lower than telecommunication satellites. A similar, but less marked behaviour, can be noted by comparing crowded and uncrowded

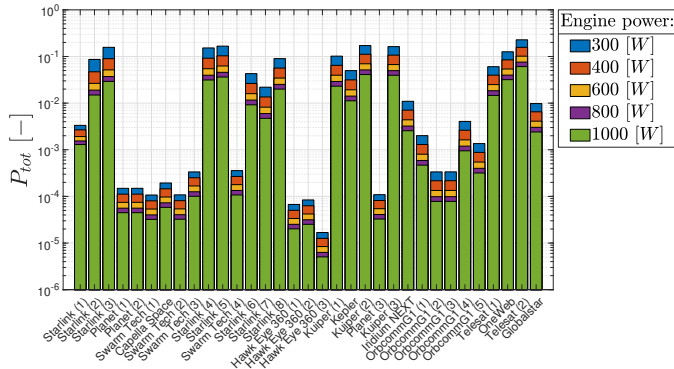


Fig. 12. Collision probability related to the replacement of the whole constellation at different engine input powers considering scenario **B**.

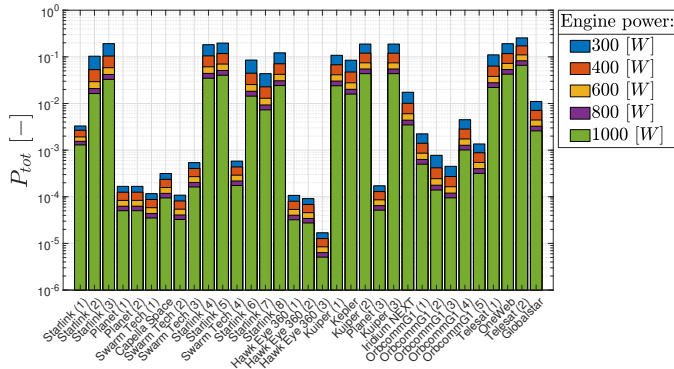


Fig. 13. Collision probability related to the replacement of the whole constellation at different engine input powers considering scenario **N**.

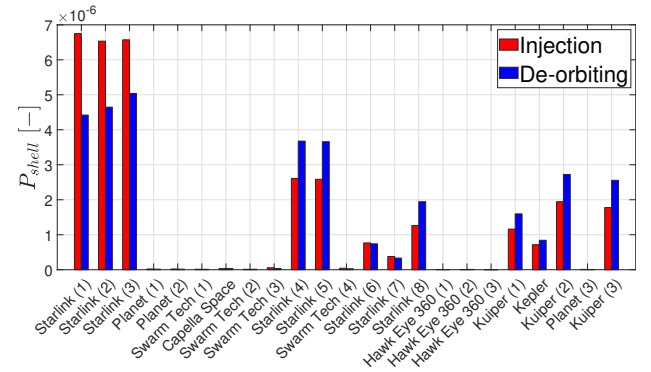


Fig. 14. Collision probability with each lower altitude constellation of one injecting and de-orbiting Kuiper (3) satellite with an engine input power of 600 W.

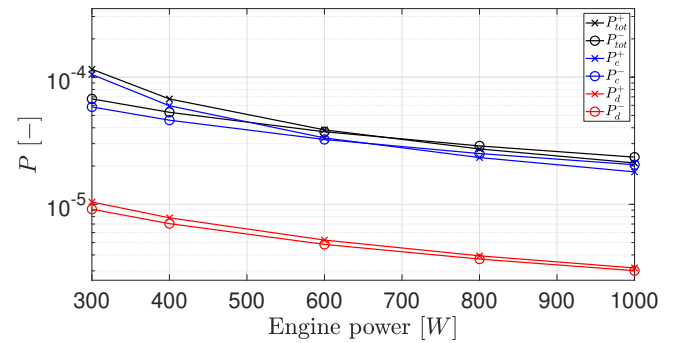


Fig. 15. Collision probability per source and engine input power of one injecting and de-orbiting Kuiper (3) satellite. Optimal injection and nominal de-orbiting have been considered.

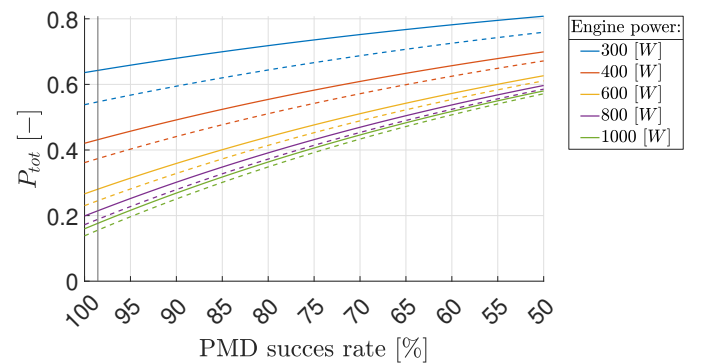


Fig. 16. Overall collision probability related to the replacement of all 11926 Starlink satellites at different PMD success rates considering both scenarios **N** (continuous) and **B** (dashed).

telecommunication shells.

Besides the benefits of a powerful thruster, it can be noticed from Fig. 16 that the PMD declared by Starlink does not substantially change the risk assessment with respect to the case of 100 % PMD success rate. Nevertheless, it must be emphasised that collisions with satellites belonging to the departure or arrival shell are not contemplated.

Considering Fig. 14, a satellite on its journey has a higher chance of colliding with a constellation satellite, rather than with a debris. On the other hand, constellation satellites can be tracked much more easily and, unlike debris, are manoeuvrable.

By looking at Fig. 15 it is also clear that the Starlink shells in Very-Low Earth Orbit (VLEO) pose the greatest threat. The large gap between injection and de-orbiting collision probabilities is due to the low altitude of the shells, at which the atmospheric drag is considerable, as drag accelerates de-orbiting while slowing down injection. Moreover, by looking at Figs 12 and 13, the collision probability for the replacement of Starlink VLEO shells is comparable to higher altitude shells, even if they have to go through far fewer shells. The reason for this is the large number of satellites that VLEO shells require to ensure (near) global coverage, thus creating a thin region of space heavily populated. On the other hand, it must be emphasised that the lower the altitude of the shell, the faster the re-entry of the debris generated from an in-orbit collision.

A final remark shall be made about the size of the satellites. Indeed, the collision probabilities considering spherical shapes are, in general, larger than the actual values. This issue is treated in Le May et al. (2018), where it is shown that the average number of collisions between space debris and one Starlink satellite modeled as a sphere, is around 8 % larger than the one computed using a box wind model.

6. Preliminary analysis of the consequences of an in-orbit catastrophic collision

In the following, a risk assessment related to the interaction between satellite constellations and a cloud of fragments, generated by an in-orbit catastrophic collision, will be performed. The model developed in Section 2 will be used for the evaluation of the collision probability between each generated fragment that, due to its passive de-orbiting, has to cross lower altitude satellite constellations.

6.1. Methodology

NASA standard breakup model, described in Johnson et al. (2001), has been utilised for the evaluation of the area-to-mass ratio A/M and area A of the fragments, having characteristic lengths between 2 cm and 2 m. This interval of characteristic lengths has been divided into 100 logarithmic bins for the evaluation of the total number of fragments N_f , as done similarly in Letizia (2016). Assuming spherical shaped fragments, both the radius R and the mass M can also be determined.

As discussed in Jehn (1991), Ashenberg (1994) and Letizia et al. (2015), Earth's oblateness spreads the fragments along the

argument of periapsis ω and RAAN Ω . At this point, again according to Letizia et al. (2015), the Keplerian parameters can be randomised and the only perturbing acceleration that has to be accounted for the propagation of the fragments is atmospheric drag.

In this study, the risk assessment of every shell-crossing event is performed by assuming that each fragment has an inclination i_2 equal to the one of the satellite they have been generated from, and RAAN Ω_2 which is uniformly randomised between 0° and 360° .

Furthermore, the collision angles φ_i between a crossing object and each constellation's orbital plane are quite spread, since they are equally spaced along the RAAN. The randomisation of the collision angles would, therefore, provide good statistical results if used for hundreds of thousands of shell-crossing events, as it is the case for the risk assessment of a debris cloud crossing a shell.

The covariance matrices of the fragments are modeled as diagonal in their respective RSW frames, with fixed axes ratios and randomised determinant:

$$\zeta^{RSW} = \rho \begin{bmatrix} 1 & 0 & 0 \\ 0 & 4 & 0 \\ 0 & 0 & 1 \end{bmatrix}, \quad 5 \leq \rho \leq 10 \quad (54)$$

It was observed that neglecting the covariance matrices and using Eq. (43) produces the same results, since for most orbit orientations, the condition $\varphi \leq \varphi^*$ holds.

Depending on the physical properties of fragments and constellations' satellites, it can be determined whether an eventual collision would be catastrophic or non-catastrophic, and the debris trackable or non-trackable. The former distinction is solved using a statistical approach (Polli, 2021). Fragments with mass equal or greater than a threshold value M_p^* are considered to cause a catastrophic collision. The critical mass is defined as:

$$M_p^* = \frac{E_k M_1 a_1}{\mu(1 - \cos i_1 \cos i_2)} \quad (55)$$

where M_1 is the mass of the target satellite and $E_k = 40 \frac{\text{J}}{\text{g}}$ is the minimum impact energy per target mass necessary for a collision to be catastrophic (Krisko, 2007). A length of 10 cm (Radtke et al., 2017) has been chosen as a threshold value between trackable and non-trackable objects.

Finally, in Letizia (2016) a simulation was carried of a non-catastrophic collision characterised by an impact energy of 50 kJ. It was shown that almost every fragment has an eccentricity between 0 and 3×10^{-1} , half of which are lower than 5×10^{-2} . For this reason, the results collected in Section 6.2 are yet to be completely validated.

6.2. Results

Two different scenarios have been considered: a catastrophic collision between a 200 kg Starlink (8) satellite and a 10 kg debris; a catastrophic collision between two 200 kg Starlink (8) satellites.

The collision probabilities between each fragment and each shell crossed are shown in Figs 17 and 18. The black dots refer

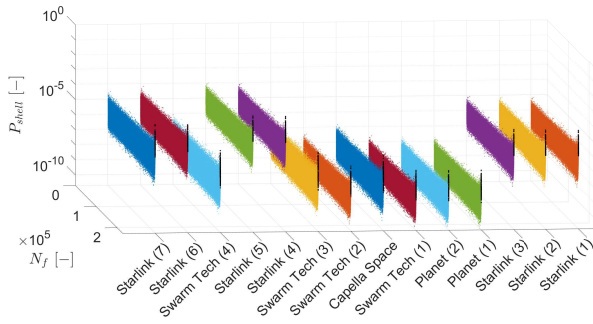


Fig. 17. Collision probabilities of the Starlink-debris collision cloud per shell and fragment. Fragments are sorted based on their characteristic lengths.

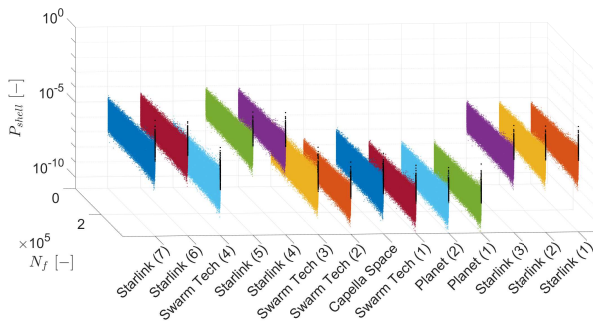


Fig. 18. Collision probabilities of the Starlink-Starlink collision cloud per shell and fragment. Fragments are sorted based on their characteristic lengths.

to catastrophic collision probabilities. These probabilities are in general larger than the non-catastrophic collision probabilities, as catastrophic collision are caused by heavy fragments, which, usually, have large cross-sectional areas.

As collisions with trackable objects can be prevented much more easily, only results about collision probabilities with non-trackable debris are shown in Fig. 19.

Non-trackable non-catastrophic collisions are the main threat posed by a fragmentation event. Although catastrophic collisions result in the total disruption of the target, small objects are, in general, more numerous and they would not only contribute to the generation of more fragments, but also damage the impacting satellite, thus increasing the failure rate. Due to their smaller mass, Earth observation satellites have a relatively higher chance of a non-trackable catastrophic collision.

The results obtained show that an in-orbit collision would most probably decree LEO inoperability due to cascade effect. Nonetheless, the dynamics involved in this type of shell-crossing events are, in general, very slow, thus granting a large time window to operate. Indeed, the higher the altitude at which the catastrophic collision may occurs, the slower the dynamics of the satellite, the easier preventing collisions. On the other hand, the higher the collision altitude, the longer the time needed for the disposal of the debris cloud.

Finally, to highlight the performances of the model, using a single core of an i7-4720 at 2.6 GHz with 8 GB of RAM, the risk assessments of the Starlink-debris and Starlink-Starlink

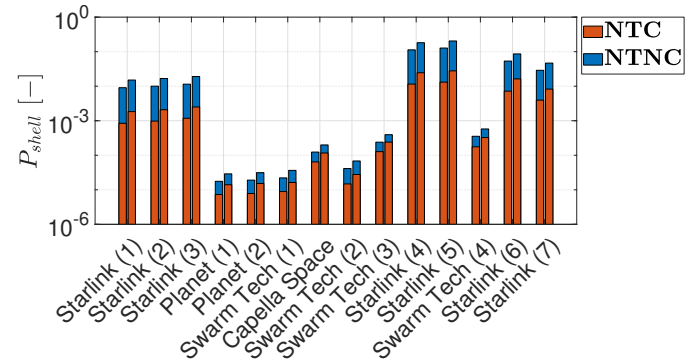


Fig. 19. Collision probability per shell of non-trackable catastrophic (NTC) and non-trackable non-catastrophic (NTNC) collisions considering fragments from Starlink-debris (left) and Starlink-Starlink (right) collision.

collision scenarios required MATLAB 20.57 and 33.55 seconds, respectively. In this time windows, a total of 3,184,398 and 5,163,074 shell-crossing events were analysed.

7. Conclusion

This study has proposed an analytical model for the assessment of the environmental threat posed by large satellite constellations, through a statistical modeling of the collision probability related to a shell-crossing event. The main advantage of the statistical model is the low computational effort, as the collision probability related to millions of shell-crossing events can be assessed within seconds on an average personal computer. The model was used to analyse the constellations replacement traffic and the consequences of an in-orbit catastrophic collision.

Constellation's satellites have to be replaced once they reach their EoL, thus generating an intense traffic in LEO. Both injection and disposal have been investigated, showing that, besides phasing, the main parameters of interest are the semi-major axis rate of change $|\Delta a|$ and the relative orientations between the constellation's and crossing orbital planes, summarised by the collision angle φ . As $|\Delta a|$ can be tuned through the proper selection of the satellite's thruster, a great emphasis was placed in the design of an optimal crossing orbit, which was found to be at zero inclination. The establishment of an international gateway orbital corridor for both injection and disposal might simplify the management of future space traffic scenarios, as satellites on the same orbits share the lowest possible probability that a collision will occur.

In the context of constellation replacements, an analysis of the risk assessment based on different PMD success rates has also been performed regarding the Starlink constellation. The results proved that the benefits arising from the selection of a powerful thruster are much greater than the ones arising from the decrease of the failure rate, proving once again that the main parameters of interest for the design of a shell-crossing manoeuvre is the semi-major axis rate of change.

The statistical model has also been used for the risk assessment

of the debris flux generated from an in-orbit catastrophic collision. With emphasis on the probability of a collision with non-trackable objects, it was shown that, considering the presence of thousands of constellation's satellites, managing the consequences of a collision is definitely an arduous task.

Although the statistical model presented in Section 2 was developed based on the assumption of circular orbits, it was shown that the mean collision probability can be predicted with great accuracy for crossing orbit eccentricity e_2 up to 10^{-3} . More elliptical crossing orbits are yet to be tested. It was also shown that low eccentricity crossing orbits allow for a greater collision probability minimisation, through proper phasing between satellites.

The main limitation of the model is that its reliability is not proven when the effects of J_2 perturbations are considered. Furthermore, the model is specifically designed for assessments of traffic scenarios and preliminary mission analysis, as the result is an estimation of the average collision probability, whereas the propagation method showed that the true anomaly phase between constellation's and crossing satellite is a parameter of great interest for the design of shell-crossing events.

The analysis of the limitations of this study has already suggested the main topics for possible future improvements. Indeed, the main focus would be to test the accuracy of the model in case of more elliptical crossing orbits, also including J_2 in the analysis. Another possibility would be to develop a semi-analytical model with the possibility of using covariance matrices not necessarily diagonal in their respective RSW frames. Finally, it is possible to analyse the collision probability profile $P(\delta\omega^{(0)})$ of a shell-crossing event in the frequency domain. This might be a convenient choice for the development of an analytical model, able to retrieve the collision probability profile based on the main parameters of the shell-crossing event, thus avoiding numerical methods exploitation.

8. Acknowledgements

This project has received funding from the European Research Council (ERC) under the European Union's Horizon 2020 research and innovation programme [grant agreement No 679086 – COMPASS].

References

- Alfano, S. (2002). *Aerospace support to space situation awareness*. Presentation at MIT Lincoln Laboratory Satellite Operations and Safety Workshop, Haystack Observatory, Chelmsford, Massachusetts, United States of America, October.
- Ashenberg, J. (1994). Formulas for the phase characteristics in the problem of low-earth-orbital debris. *Journal of Spacecraft and Rockets*, 31(6), 1044–1049. doi:10.2514/3.26556.
- Bai, X.-Z., Chen, L., & Tang, G.-J. (2013). Explicit expression of collision probability in terms of RSW and NTW components of relative position. *Advances in Space Research*, 52(6), 1078–1096. doi:10.1016/j.asr.2013.05.034.
- Battin, R. H. (1999). *An Introduction to the Mathematics and Methods of Astrodynamics*. American Institute of Aeronautics and Astronautics, New York, New York, United States of America. doi:10.2514/4.861543.
- Chan, F. K. (2008). *Spacecraft Collision Probability*. The Aerospace Corporation, El Segundo, California, United States of America. doi:10.2514/4.989186.
- FCC (2008). Orbcomm G1: order and authorization. URL: <https://www.fcc.gov/document/orbcomm-license-corp>.
- FCC (2011). Globalstar: attachment schedule S GXT. URL: <https://fcc.report/IBFS/SAT-MOD-20080904-00165>.
- FCC (2013). Planet: technical and operational description. URL: <https://fcc.report/IBFS/SAT-MOD-20140321-00032/1040242.pdf>.
- FCC (2016). Iridium: application for mobile satellite service. URL: <https://fcc.report/IBFS/SAT-MOD-20131227-00148>.
- FCC (2017). HawkEye 360: technical informations. URL: <https://apps.fcc.gov/els/GetAtt.html?id=186546&x>.
- FCC (2018). Swarm Tech: narrative exhibit. URL: https://licensing.fcc.gov/myibfs/download.do?attachment_key=1592875.
- FCC (2018-2021). Starlink: attachment menu. URL: https://licensing.fcc.gov/cgi-bin/ws.exe/prod/ib/forms/attachment_menu.htm?id_app_num=133714&acct=599269&id_form_num=15&filing_key=-443498.
- FCC (2019). Kuiper: technical appendix. URL: <https://fcc.report/IBFS/SAT-LOA-20190704-00057/1773885>.
- FCC (2020a). OneWeb: application for modification. URL: <https://fcc.report/IBFS/SAT-MPL-20200526-00062/2379569.pdf>.
- FCC (2020b). Telesat: application for modification of market access authorization. URL: <https://fcc.report/IBFS/SAT-MPL-20200526-00053/2378318.pdf>.
- Foster, J. L., & Estes, H. S. (1992). *A parametric analysis of orbital debris collision probability and maneuver rate for space vehicles*. National Aeronautics and Space Administration, Houston, Texas, United States of America.
- García-Pelayo, R., & Hernando-Ayuso, J. (2016). Series for collision probability in short-encounter model. *Journal of Guidance, Control, and Dynamics*, 39(8), 1904–1912.
- Gronchi, G. F. (2005). An algebraic method to compute the critical points of the distance function between two Keplerian orbits. *Celestial Mechanics and Dynamical Astronomy*, 93(1), 295–329. doi:10.1007/s10569-005-1623-5.
- Huang, S., Colombo, C., & Bernelli-Zazzera, F. (2021). Multi-criteria design of continuous global coverage walker and street-of-coverage constellations through property assessment. *Acta Astronautica*, 188, 151–170.
- Jehn, R. (1991). Dispersion of debris clouds from on-orbit fragmentation events. *ESA Journal*, 15(1), 63–77.
- Johnson, N. L., Krisko, P., Liou, J.-C. et al. (2001). NASA's new breakup model of evolve 4.0. *Advances in Space Research*, 28(9), 1377–1384. doi:10.1016/S0273-1177(01)00423-9.
- Kramer (2021). Starlink satellite constellation of SpaceX. URL: <https://directory.eoportal.org/web/eoportal/satellite-missions/s/starlink>.
- Kramer, H. J. (2019). Capella Space: order and authorization. URL: <https://directory.eoportal.org/web/eoportal/satellite-missions/content/-/article/capella-x-sar>.
- Krisko, P. H. (2007). The predicted growth of the low-earth orbit space debris environment—an assessment of future risk for spacecraft. *Proceedings of the Institution of Mechanical Engineers, Part G: Journal of Aerospace Engineering*, 221(6), 975–985. doi:10.1243/09544100JAERO192.
- Le May, S., Gehly, S., Carter, B. et al. (2018). Space debris collision probability analysis for proposed global broadband constellations. *Acta Astronautica*, 151, 445–455. doi:10.1016/j.actaastro.2018.06.036.
- Letizia, F. (2016). *Space debris cloud evolution in Low Earth Orbit*. Ph.D. thesis University of Southampton. doi:10.13140/RG.2.1.3817.7047.
- Letizia, F., Colombo, C., & Lewis, H. G. (2015). Analytical model for the propagation of small-debris-object clouds after fragmentations. *Journal of Guidance, Control, and Dynamics*, 38(8), 1478–1491. doi:10.2514/1.6000695.
- Patera, R. (2000). A general method for calculating satellite collision probability. *Advances in the astronautical sciences*, 105(2), 1275–1290. doi:10.2514/2.4771.
- Pollard, J. E. (1998). Evaluation of low-thrust orbital maneuvers. In *34th AIAA/ASME/SAE/ASEE Joint Propulsion Conference and Exhibit* (pp. AIAA-98-3486). American Institute of Aeronautics and Astronautics, Cleveland, Ohio, United States of America, 13–15 July. doi:10.2514/6.1998-3486.

- Pollard, J. E. (2000). *Simplified analysis of low-thrust orbital maneuvers*. Technical Report The Aerospace Corporation, El Segundo, California, United States of America.
- Polli, E. M. (2021). *Statistical analysis of environmental impact of satellite constellations*. Master's thesis Politecnico di Milano. URL: <https://www.politesi.polimi.it/handle/10589/175669>.
- Radtko, J., Kerschull, C., & Stoll, E. (2017). Interactions of the space debris environment with mega constellations—using the example of the OneWeb constellation. *Acta Astronautica*, 131, 55–68. doi:10.1016/j.actaastro.2016.11.021.
- Rossi, A., Alessi, E., Valsecchi, G. et al. (2017). A quantitative evaluation of the environmental impact of the mega constellations. In *7th European conference in space debris*. The European Space Agency (ESA), Darmstadt, Germany, 18–21 April.
- Rossi, A., Anselmo, L., Pardini, C. et al. (1998). Interaction of the satellite constellations with the low earth orbit debris environment. In *Mission Design & Implementation of Satellite Constellations* (pp. 327–335). Springer. doi:10.1007/978-94-011-5088-0_29.
- Serra, R., Arzelier, D., Joldes, M. et al. (2016). Fast and accurate computation of orbital collision probability for short-term encounters. *Journal of Guidance, Control, and Dynamics*, 39(5), 1009–1021.
- UCS (2022). UCS satellite database. URL: <https://www.ucsusa.org/resources/satellite-database>.
- Walker, J. G. (1984). Satellite constellations. *Journal of the British Interplanetary Society*, 37, 559–571.